Magnetostructural Coupling Drives Magnetocaloric Behavior: The Case of MnB versus FeB

Joshua D. Bocarsly,[†,‡] Emily E. Levin,[†,‡] Samuel A. Humphrey,[¶] Tom Faske,[§] Wolfgang Donner,[§] Stephen D. Wilson,[†,‡] and Ram Seshadri[*,†,‖,‡]

†*Materials Department*

University of California, Santa Barbara, California 93106, United States

‡*Materials Research Laboratory*

University of California, Santa Barbara, California 93106, United States

¶*Department of Materials*

University of Oxford, Oxford OX1 3PH, United Kingdom

§*Department of Materials and Earth Sciences, Technische Universität Darmstadt, Darmstadt 64287, Germany.*

‖*Department of Chemistry and Biochemistry*

University of California, Santa Barbara, California 93106, United States

E-mail: seshadri@mrl.ucsb.edu

Abstract

Materials with strongly coupled magnetic and structural transitions can display a giant magnetocaloric effect, which is of interest in the design of energy-efficient and environmentally-friendly refrigerators, heat pumps, and thermomagnetic generators. There also exist however, a class of materials with no known magnetostructural transition that nevertheless show remarkable magnetocaloric effects. MnB has been recently suggested as such a compound, displaying a large magnetocaloric effect at its Curie temperature (570 K) showing promise in recovering low-grade waste heat using thermomagnetic generation. In contrast, we show that isostructural FeB displays very similar magnetic ordering characteristics, but is not an effective magnetocaloric. Temperature- and field-dependent diffraction studies reveal dramatic magnetoelastic coupling in MnB, which exists without a magnetostructural transition. No such behavior is seen in FeB. Furthermore, the magnetic transition in MnB is shown to be subtly first-order, albeit with distinct behavior from that displayed by other magnetocalorics with first-order transitions. Density functional theory-based electronic structure calculations point to the magnetoelastic behavior in MnB as arising from a competition between Mn moment formation and B–B bonding.

Introduction

While the Curie transition from a paramagnet to a ferromagnet is canonically a continuous transition, there exist ferromagnets that display discontinuous first-order transitions. This phenomenon can arise when magnetic and structural degrees of freedom are so strongly coupled that the magnetic phase transition is accompanied by a structural transition. Materials displaying such coupled transitions, including MnAs,[1,2] ferromagnetic, hole-doped $LaMnO_3$,[3] $Gd_5(Si, Ge)_4$,[4–8] $(Mn,Fe)_2(P,Si,Ge,As)$,[9–13] and $La(Fe,Si)_{13}H_x$[14,15] are of great interest for their unusual functionality, including, variously, colossal magnetoresistance, giant magnetovolume effects, and, most recently, giant magnetocaloric effects. The magne-

tocaloric properties stem from the fact that this type of first-order transition can often be actuated using a modest magnetic field, leading to relatively small fields ordering a significant fraction of paramagnetic spins. By alternating cycles of adiabatic and isothermal magnetization and demagnetization, these changes in entropy can be leveraged to drive an environmentally-friendly and energy-efficient heat pump.[16] Conversely, changes of temperature can be employed to build efficient thermomagnetic waste heat regenerators.[17–19] The primary metric for magnetocaloric performance is the peak entropy change that can be accomplished during isothermal application of a given magnetic field, $\Delta S_{M,\mathrm{peak}}(H)$. For commercial applications, earth-abundant materials that have substantial peak isothermal magnetic entropy changes at low fields (*ie.* $H = 1\,\mathrm{T}$ to $2\,\mathrm{T}$) are attractive.

Giant first-order magnetostructural phase transitions are recognized by the usual hallmarks of an abrupt change in the magnetization at the transition temperature accompanied by a peak in heat capacity, thermal hysteresis, and phase coexistence of the two phases at the transition temperature. The structural phase transition may either be from one crystallographic space group to another (*e.g.* the $P6_3/mmc$ to $Pnma$ transition seen in MnAs[2]), or it may involve two phases within the same structure but with distinct lattice parameters (*e.g.* the transition in $(Fe,Mn)_2(P,Si)$[20]). The latter case is often termed a magnetoelastic transition.

While the giant magnetic entropy changes associated with first-order magnetostructural phase transitions are useful in applications, they pose engineering challenges. The thermal and magnetic hysteresis associated with first-order transitions leads to inefficiencies and rate limitations when the material is cycled between magnetic states. Large changes in structure during cycling can lead to fatigue and mechanical degradation. Furthermore, thermal hysteresis greatly reduces the reversible adiabatic temperature change of a magnetocaloric. While these challenges can often be alleviated using chemical tuning and device engineering,[21–23] a different solution that has gained popularity recently is to change the composition of a first-order material in order to weaken the magnetostruc-

tural coupling so that the transition becomes increasingly second-order. At the border between first- and second-order transitions, one may find a tricritical transition which has no hysteresis while maintaining a large ΔS_M.[12,20,24–27] In contrast, for systems without magnetostructural first-order transitions, the main strategy for improving ΔS_M has been to increase the magnetic moment.[28–30] However, there exist several materials such as $AlFe_2B_2$,[31,32] Mn_5Ge_3,[33] CrO_2,[34] MnCoP,[35] and MnB[35,36] which show promising magnetocaloric properties without any known first-order magnetostructural or magnetoelastic transitions. All of these materials have ΔS_M values that are competitive with, or exceed that of Gd metal despite having gravimetric magnetic moments at saturation that are only between 30 % and 60 % as large.[37] All these materials also have large values of magnetic deformation Σ_M, a density functional theory-based indicator of the strength of magnetostructural coupling,[35] suggesting that magnetostructural coupling may play an underappreciated role in the good magnetocaloric properties of these materials.

Here, we present the case study of MnB *vs.* FeB to demonstrate that magnetostructural coupling is the driving force behind a large magnetocaloric effect, even in a system with no obvious first-order magnetostructural transitions. MnB and FeB are both ferromagnets with the same structure (FeB-type, shown in Figure 1) and comparable magnetic properties, but MnB has a large ΔS_M of $-10.7\,\mathrm{J\,kg^{-1}\,K^{-1}}$ for an applied field of 5 T while FeB has an effect three times smaller. Interestingly, some anomalous structural behavior near the Curie temperature of MnB was reported as early as 1975.[38,39] However, this phenomenon was not explained, and MnB has not received much attention until recently.[35,36,40–42]

We use high-resolution temperature-dependent synchrotron powder diffraction and diffraction under a magnetic field to study the magnetostructural coupling in MnB and FeB. We find that despite the similarities between the two compounds, MnB shows dramatic anisotropic coupling between its lattice and magnetism while FeB does not. We employ density functional theory calculations to understand the origin of this magnetostructural coupling as a competition between manganese moment formation (and the

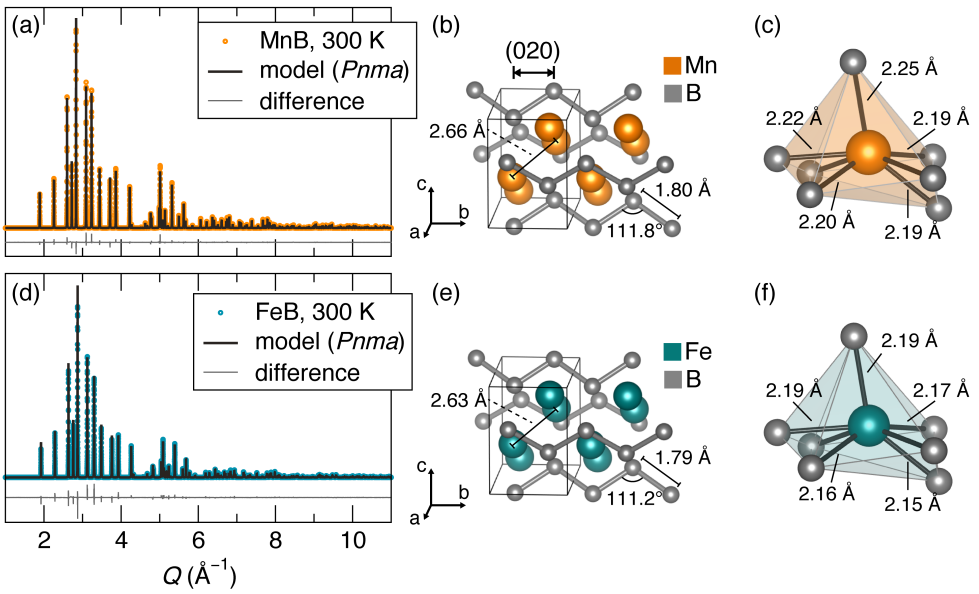

Figure 1: Crystal structures at 300 K of MnB (a-c) and FeB (d-f) determined from high-resolution synchrotron X-ray diffraction. (a) and (c) show the diffraction patterns, along with their Rietveld refinement fits. Both samples have the "FeB" structure (space group $Pnma$, no. 62) consisting of tightly bonded 1-D chains of B atoms with the metal ions arranged around them, as can be seen in (b) and (e). The B–B chain is almost unchanged between the structures, but slightly larger Mn-B contacts lead to the MnB cell having a 4.3% larger unit cell volume. The difference in a, b, and c lattice parameters are 1.1%, 0.97%, and 2.2%, respectively. Refined structures are provided in the Supporting Information as Crystallographic Information Files.

associated volume effects) and B–B bonding. This competition leads MnB to be delicately balanced between competing magnetic and structural considerations, yielding a system where a small stimulus can drive large changes in structure and magnetism. Furthermore, we determine the magnetic transition in MnB is in fact subtly first-order, as revealed by phase coexistence between two isostructural phases with slightly different lattice parameters at the magnetic transition temperature. However, this subtly first-order transition appears to be distinct from the giant magnetostructural or magnetoelastic transitions seen in other magnetocalorics. The present observation is enabled by the very high resolution of the synchrotron diffraction experiments. We propose that similar behavior may also be revealed in other magnetocaloric compounds if they were to be examined in similar resolution.

Materials and methods

Phase-pure powders of MnB and FeB were prepared by assisted microwave synthesis, as reported previously.[35] Briefly, Mn (Alfa Aesar, 99.95%) or Fe (Aldrich, 99.9%) powders were ground in air with 2 % stoichiometric excess of crystalline B powder (Alfa Aesar, 99.5%), pressed into pellets, and sealed in evacuated silica ampoules. The ampoules were placed in a carbon-filled crucible and heated in a 1200 W domestic microwave oven (Panasonic, model NN-SN651B) at 70% power (840 W) for 3 min. The pellets were then annealed in evacuated ampoules at 1100°C for 2 days, followed by air quenching. The samples were confirmed to be phase-pure MnB or FeB prior to and after the final anneal. The excess B required is believed to be due to incomplete reaction of the boron starting material. The samples showed no signs of oxidation or air-sensitivity, and are treated as air stable.

Magnetic measurements were performed on a Quantum Design Physical Property Measurement System (PPMS DynaCool) equipped with a Vibrating Sample Magnetometer (VSM) oven option which allows for the collection of magnetic data between 300 K and 1000 K. The magnetocaloric isothermal entropy change upon magnetization ($\Delta S_M(H,T)$) for each sample was determined using the appropriate Maxwell relation, from magnetization M *vs.* T measurements taken while sweeping temperature through the magnetic transition at several fixed magnetic fields between H = 0.1 T and H = 5 T. The temperature derivatives of magnetization were calculated using Tikhonov regularization,[43] as described in detail previously.[44] Raw measurement data are presented in the Supporting Information Figure S1.

High-resolution synchrotron powder diffraction data were collected on Beamline 11-BM at the Advanced Photon Source (APS), Argonne National Laboratory using an average wavelength of 0.414581 Å. Room temperature data were collected between 2θ of 0.5° and 50°. Temperature-dependent data was collected between 0.5° and 34° for MnB (10 minute collection time per pattern), and betwen 0.5° and 28° for FeB (5 minute collection time per pattern). A calibrated Cyberstar Hot Gas Blower was used to control the temperature.

Patterns were collected continually while temperature was ramped slowly cooled through the magnetic transition such that one diffraction pattern was taken at every 3 K interval. Resulting patterns were refined using Topas Academic, using sequential and parametric[45] refinement.

Temperature and magnetic-field dependent X-ray powder diffraction measurements were performed on a custom-built laboratory diffractometer in transmission geometry (Mo Kα radiation, $\lambda_1 = 0.709320$ Å, $\lambda_2 = 0.713317$ Å, using the 2θ range from 7° to 67° with a step size of 0.0097°). The instrument has been described in detail elsewhere.[46] The sample powder was mixed with NIST 640d standard reference silicon for correction of geometric errors. Temperature in the range from 300 K to 700 K was controlled by means of a custom SHI closed-cycle Helium cryofurnace. The heating rate between the measurements was 10 K min^{-1} and the sample temperature was stabilized for 15 min. before data collection. Magnetic fields of up to 5 T were applied for isofield warming and cooling protocols, as well as for isothermal field-application experiments. Pawley analyses of the obtained diffraction patterns were carried out sequentially using TOPAS Academic. Example data and fits are available in the Supporting Information Figures S6 and S7.

Spin-polarized density functional theory calculations were performed using the Vienna Ab initio Simulation Package (VASP)[47] using projector augmented wave (PAW) pseudopotentials[48,49] within the Perdew-Burke-Ernzerhof (PBE) generalized gradient approximation (GGA).[50] First, the eight-atom unit cells of MnB and FeB were relaxed with a force convergence of 0.001 eV Å^{-1} and a starting magnetic moment of 3 μ_B per transition metal ion. This resulted in lattice parameters a, b, c of 5.36, 2.96, and 4.07 Åfor MnB and 5.32, 2.93, and 3.96 Åfor FeB, which are within reasonable agreement of the room temperature lattice parameters given in Supporting Information Table S1. Based on these structures, unit cells with systematically expanded and contracted b lattice parameters were generated and ion-only relaxations were performed. On these relaxed structures, static spin-polarized and nonspin-polarized calculations were performed. The Crystal Orbital Hamilton Population

(COHP) between pairs of B atoms in the chain were calculated with the help of the LOBSTER code.[51–55]

Results and Discussions

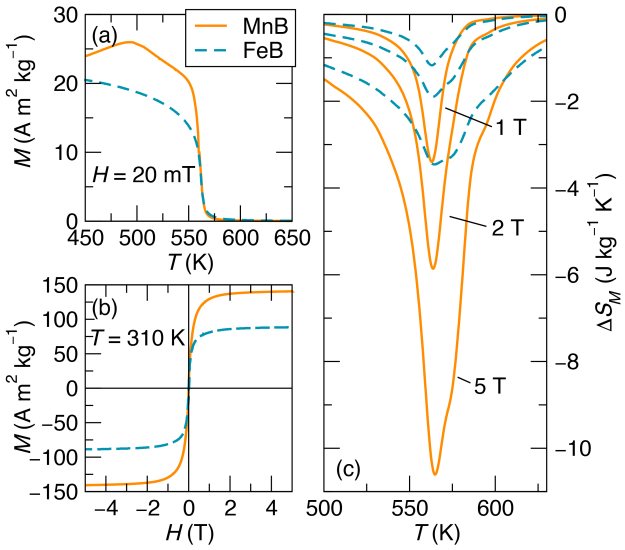

Figure 2: Comparison of the magnetism of MnB and FeB. (a) The two materials show a nearly identical magnetic transition temperature, but MnB shows an unconventional shape of the $M(T)$ curve. (b) MnB has a saturation magnetization about 50% larger than that of FeB, (c) but shows a peak $-\Delta S_M$ about three times larger.

The results of Rietveld refinement of high-resolution MnB and FeB patterns collected at room temperature are shown in Figure 1 and Table S1. Both patterns match the known orthorhombic $Pnma$ structure ("FeB-type"),[56,57] which consists of 1D zigzag chains of closely spaced (1.8 Å) B atoms running along the b crystallographic axis with Mn or Fe arranged in a distorted hexagonal network around these chains. This results in a highly bonded framework, with each metal atom coordinated by seven boron atoms within a sphere of 2.3 Åand six additional metal atoms within 2.7 Å. These diffraction patterns display anisotropic peak widths, which can be well-fit using the Stephens peak-shape function[58] which accounts for (hkl)-dependent peak broadening by assuming that different crystallographic directions may have different amounts of inhomogenous strain. The anisotropy in peak shape is

consistent with the highly one-dimensional nature of the crystal structure.

MnB and FeB show very similar bond lengths and contacts, albeit with slightly larger metal-B contacts in MnB leading to larger lattice parameters and a 4.3% larger unit cell volume for MnB. It should be noted the B–B bond lengths and the lattice parameter in their direction of propagation are very similar in the two materials.

Figure 2 shows the magnetic characterization of pure samples of MnB and FeB. MnB and FeB show remarkably similar magnetic ordering temperatures (560 K), despite the magnetic behavior appearing to display some key differences. Under low applied fields (less than about 0.1 T), M *vs.* T of FeB behaves as expected for a ferromagnet, uniformly increasing as temperature is lowered. MnB on the other hand, shows an atypical maximum in the magnetization around 500 K, whose origin is not known but may represent a spin reorientation or other magnetic transition. The gravimetric saturated magnetic moment of MnB is about 50% larger than that of FeB (1.65 $\mu_{\mathrm{B}}/\mathrm{Mn}$ and 1.05 $\mu_{\mathrm{B}}/\mathrm{Fe}$). This difference in saturated moment is not nearly enough to explain the dramatic difference in the magnetocaloric properties, with MnB showing a three times larger magnitude of peak ΔS_M. No resolvable thermal hysteresis was seen in either material.

The large ΔS_M in MnB compared to FeB is surprising, given the similarities in structure, ordering temperature and ordered magnetic moment. However, when the temperature-dependence of the synchrotron X-ray diffraction is examined (Figure 3), striking differences become evident. In FeB, all of the peaks shift uniformly towards higher Q upon cooling through the magnetic transition, demonstrating conventional positive thermal expansion. In MnB, different peaks shift in different directions, indicating highly anisotropic effects. Furthermore, pronounced kinks are visible in the thermal evolution of most of the peaks at the magnetic transition temperature, suggesting that the crystal structure is much more strongly linked to the magnetism in MnB than in FeB.

Figure 4 shows the temperature evolution of the (020) peak of the two compounds which corresponds to the lattice spacing parallel to the B–B chain direction. In MnB, this

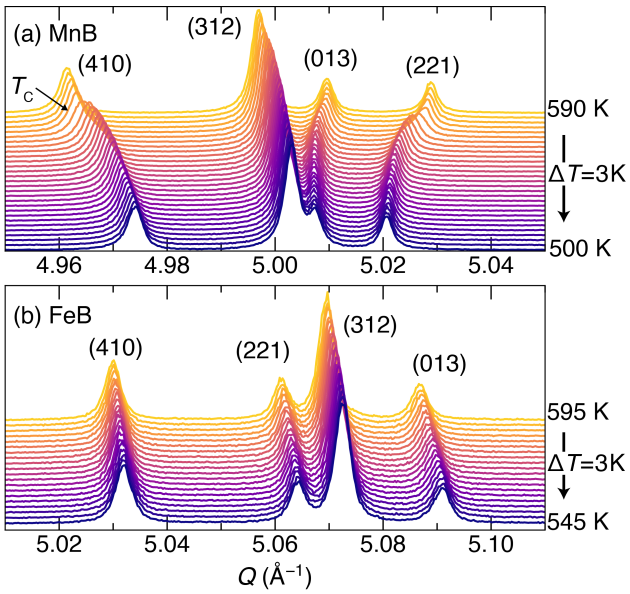

Figure 3: A section of the temperature-dependent diffraction dataset for (a) MnB and (b) FeB. MnB shows highly anisotropic thermal evolution of the diffraction peaks, including pronounced kinks at the Curie temperature. FeB, on the other hand, shows only conventional thermal expansion.

peak shifts towards lower Q upon cooling, showing a negative coefficient of thermal expansion in the b lattice parameter. Furthermore, around the magnetic transition temperature, the peak broadens dramatically and can be seen to form a distinct shoulder (Figure 4b), indicating that two closely spaced peaks are present. This effect is subtle enough that it would be undetectable at the resolution of most diffraction experiments, including laboratory X-ray diffraction or powder neutron diffraction. However, with the resolution of the present experiment, the splitting of one peak into two around the magnetic transition temperature is seen on all peaks with substantial h or k character. In addition to the data shown in 4, a pattern taken at the fixed temperature 576.1 K after temperature equilibration also shows this two-phase coexistence, confirming that it is not a transient effect (Figure S2). This behavior indicates that there is a region of phase coexistence between two phases around the magnetic transition in MnB, a hallmark that the transition is actually first-order. In FeB, on the other hand, no such behavior is observed.

In order to examine the thermal evolution of the structure, parametric Rietveld refine-

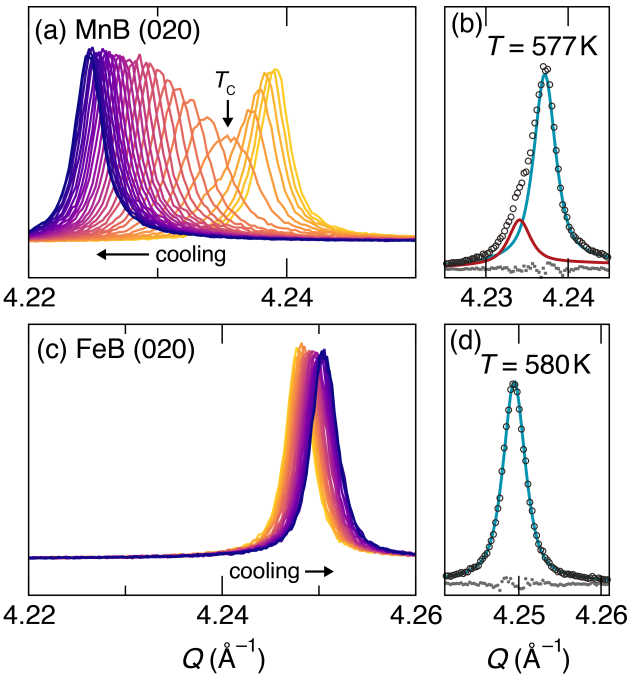

Figure 4: Temperature evolution of the (020) peak in MnB and FeB through the magnetic transition temperature. In MnB, the peak shifts dramatically to the left upon cooling (a), and broadens near the magnetic transition temperature. Below and above the magnetic transition, the peak has a well-behaved Lorentzian shape, but near the Curie temperature, it requires two peaks to fit, indicating coexistence of two phases (b). In FeB, the peak shifts to the right upon cooling (c) and maintains a constant-width Lorentzian shape at all temperatures, including at the magnetic transition temperature (d).

ments on both data sets were performed, allowing the noise in the refined parameters to be minimized. Results for FeB are shown in the Supporting Information Figure S2. The lattice parameters and unit cell volume of FeB display well-behaved linear thermal expansion of all three cell parameters, with no observable change in slope at the magnetic transition temperature. Some anisotropy is seen in the thermal expansion, with average coefficients of thermal expansion of 7 ppm K^{-1}, 12 ppm K^{-1}, and 17 ppm K^{-1} in the a, b, and c directions, respectively.

In contrast, the results of parametric refinement for MnB (Figure 5) demonstrate anomalous behavior. If the refinement for MnB is set up so that only one crystallographic phase exists in each pattern, the patterns well below and well above the transition are described appropriately, but near the transition, R_{wp} (a measure of the error in a Rietveld fit) in-

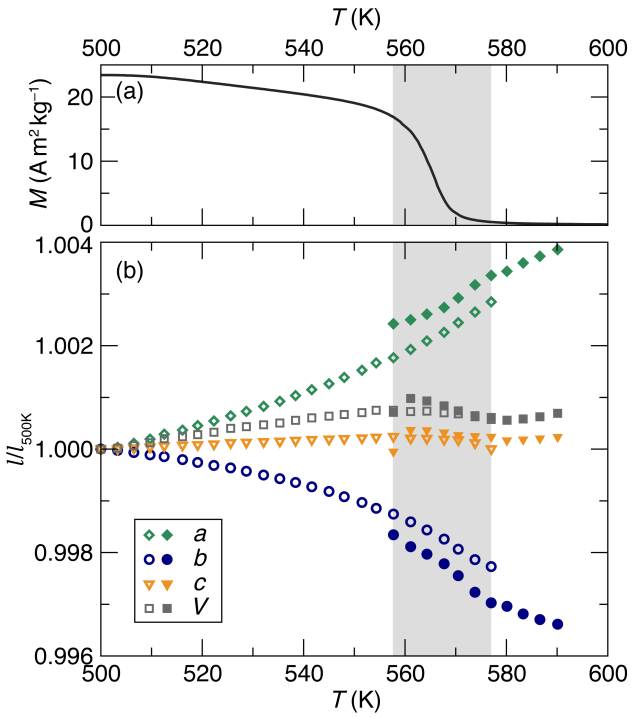

Figure 5: Results of parametric two-phase Rietveld refinement of temperature-dependent synchrotron diffraction data for MnB, compared with magnetization data. (a) Magnetization as a function of temperature under an applied field $H = 20\,\mathrm{mT}$. (b) MnB lattice parameters are shown relative to their 500 K value, and show highly anisotropic thermal expansion including large negative thermal expansion in the b direction. Furthermore, phase coexistence between two isostructural phases is seen in a 19 K window around the magnetic transition temperature, indicated with a gray box.

creases dramatically, even if the peak profile is allowed to refine independently for each temperature (Supporting Information Figure S4a). However, if two isostructural $Pnma$ phases with slightly different lattice parameters (about 0.05% difference in the a and b directions) are included in the fit, the R_{wp} remains constant across the magnetic transition. The two phases are found to coexist in a temperature region between 558 K and 577 K, transitioning from 100% of the low-temperature phase at 558 K to 100% of the high-temperature phase at 577 K (Supporting Information Figure S4b). As can be seen in Figure 5, the temperature-range of this two-phase transition corresponds exactly to the width of the magnetic transition. Taken together, these observations confirm that the magnetic transition in MnB is first-order. The phase coexistence over a temperature span

of 20 K is reminiscent of the first-order transitions in shape memory alloys, where strain buildup causes the transformation to occur progressively, rather than all at once.[59] However, it is important to note that the differences in lattice parameters of the coexisting MnB phases are not anywhere near as large as those seen in magnetocalorics displaying giant magnetocaloric effects at coupled first-order magnetostructural or magnetoelastic transitions (often 1% or more). In fact, the changes in lattice parameters between the two phases are less than the thermal expansion of each phase within the phase coexistence region, and therefore the the structural part of the phase transition cannot be considered primary. Rather, this transition appears to represent a different kind of first-order phase transition than those previously seen in magnetocalorics. Its origin and behavior are the subject of ongoing investigation.

Outside of the two-phase coexistence region, the thermal evolution of the lattice parameters of MnB is also unusual. The a lattice parameter experiences a very large positive thermal expansion across the full temperature range, with an average linear coefficient of thermal expansion of 43 ppm K^{-1} across the dataset. On the other hand, the b lattice parameter shows a similarly large negative coefficient of thermal expansion, -38 ppm K^{-1}. In the a and b directions, the positive or negative thermal expansion is strongest at the magnetic transition temperature. The c lattice parameter is relatively invariant with temperature, and the overall unit cell volume shows slight positive expansion. Both the c lattice parameter and the volume show some irregular behavior at the magnetic transition temperature.

Like the lattice parameters, the bond lengths in MnB show anisotropic thermal evolution (Supporting Information Figure S5). Notably, the closest Mn–B and B–B contacts decrease slightly as temperature is increased, as does the average Mn–Mn distance. However, the changes in bond length are all small, and with no dramatic changes at the transition temperature that would indicate a change in bond order. Rather, these anisotropic changes in bonding indicate that some electronic redistribution is occurring as temperature

is changing, as will be discussed in the final section.

The structure evolution of MnB is clearly strongly affected by the magnetism, as evidenced by the structural anomalies seen at the magnetic transition temperature. For this reason, MnB was originally compared to invar (Fe-Ni) alloys, wherein low thermal expansion is known to be caused by a magnetovolume effect.[38,39] The magnetovolume effect, which is based on theories of itinerant electron magnetism, relies on the fact that large magnetization causes lattice parameters to expand.[60,61] At low temperatures, the moment is at its largest, and its effect on expanding the crystal lattice is also at its largest. As temperature increases, fluctuations set in and the magnetic moment weakens, causing a negative contribution to the thermal expansion. This contribution may partially or completely offset the normal thermal expansion of the material due to anharmonic phonons. Above the magnetic Curie temperature, the thermal expansion typically returns abruptly to positive. In MnB however, magnetostructural effects manifest in quite a different way. The thermal expansion is marked by a change in cell shape, inducing both a strong negative thermal expansion in the b direction and a strong positive thermal expansion in the a direction. In addition, these effects persist, although somewhat weakened in magnitude, at least 150°C (see Supporting Information Figure S8) above the magnetic transition temperature, which is quite unusual, even in magnetocalorics with exceptionally large magnetostructural coupling.[46,61–63] This persistence suggests that the magnetism in MnB has at least partly local character, and that the magnetostructural interaction is related to a coupling between the moment magnitude and the Mn ion size. This coupling may persist above the Curie temperature because the local moments still exist in the paramagnetic regime.

Field Induced Magnetoelasticity

In order to directly probe magnetostructural coupling in MnB, we carried out X-ray diffraction experiments as a function of temperature under a magnetic field. Diffraction patterns

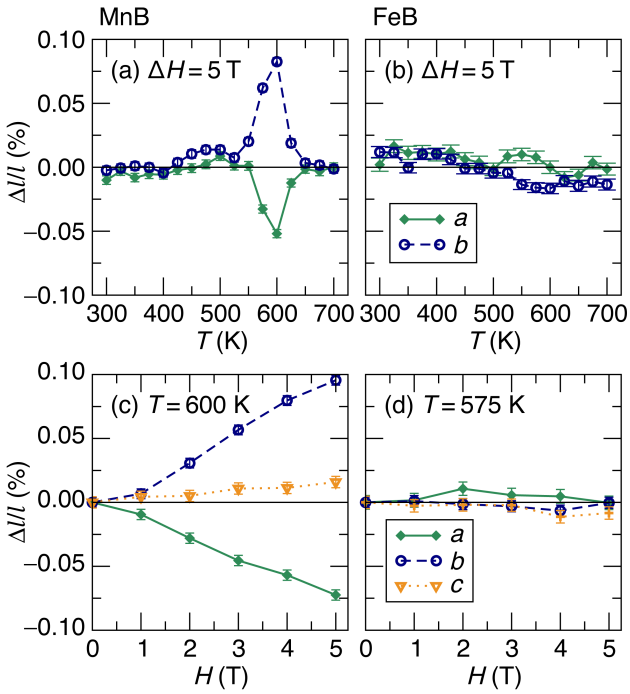

Figure 6: Changes in lattice parameters induced by magnetic field. The top row shows the relative change in lattice parameters upon application of a 5 T field, monitored as a function of temperature. (a) MnB shows large induced magnetoelasticity around its magnetic transition temperature, with a positive change in the b lattice parameter and a negative change in the a lattice parameter. No changes are clearly resolvable above the noise in FeB (b). The bottom panel shows how the lattice parameters evolve with magnetic field at fixed temperature near the magnetic transition temperature. Once again, the changes are not clearly resolved in FeB (d), but are seen to be large in MnB (c).

were collected between 300 K and 700 K under no applied field and under an applied field of 5 T. The difference in lattice parameters fit from these patterns is shown in the top panel of Figure 6. Well above and well below the transition temperature, no consistent effect can be resolved above the noise. However, near the Curie temperature where the system is most susceptible to an external field, a substantial change in lattice parameters is seen upon application of the field in MnB, an effect which we will term "induced magnetoelasticity." As with the thermal expansion, this effect is anisotropic: the a lattice parameter decreases upon application of the field, while the b lattice parameter increases by nearly 0.1 %. In FeB, no induced magnetoelasticity is resolvable. The observation of a maximum effect at 600 K in MnB as opposed to 570 K as seen in the magnetic measure-

ments and synchrotron diffraction is most likely due to the large applied field increasing the transition temperature, as well as as slight differences in the sample.

In the temperature-dependent experiment, the induced magnetoelasticity in the c lattice parameter was not determined as the c lattice parameter displayed a sample history-dependence, presumably related to the build-up and release of strains in the material. However, the induced magnetoelasticity in all three lattice parameters was resolvable in isothermal experiments, where the sample was held at a constant temperature near the magnetic transition while fields ranging from 0 T to 5 T were applied. These results are shown in the bottom row of Figure 6. Once again, no lattice parameter changes could be resolved in FeB above the noise. In MnB at 600 K, on the other hand, the b lattice parameter expands upon the application of a magnetic field, reaching a maximum expansion of 0.095(4)% (or 950 ppm) at 5 T, while the a lattice parameter contracts, reaching a contraction of $-0.072(4)$%. The c lattice parameter shows a smaller expansion, which reaches 0.016(4)%. The Q-space resolution of the in-field diffractometer is insufficient to identify the two coexisting structural phases that were seen in the synchrotron diffraction, so it is somewhat ambiguous whether these large magnetoelasticities are caused by intrinsic effects in the two coexisting phases themselves or by the field transforming part of the sample from one phase to the other. However, because the lattice parameter changes are almost twice as large as the maximum difference in lattice parameter between the two phases in the temperature-dependent synchrotron diffraction experiment, we can conclude that intrinsic magnetoelasticity in the phases is at least partially responsible for the effect. This is also consistent with a visual inspection of the diffraction patterns (Supporting Information Figure S7), which shows that the diffraction peaks shift with applied field, rather than change shape. The observed lattice parameter changes are large compared to conventional Joule magnetostriction found in all magnets (typical measured in ppm), but are smaller than values would be observed at a giant first-order magnetostructural transition (often 1% or more). This behavior positions MnB in an intermediate regime in terms of mag-

netostructural coupling, suggesting that MnB is proximal to a magnetostructural tricritical point. The explains the large, but not hysteretic ΔS_M.

This observed anisotropic magnetovolume effect in MnB explains the strange thermal expansion behavior. As MnB is heated from low temperature, its magnetic moment falls as fluctuations set in, and therefore the moment's influence on structure is decreased. On the other hand, when an external magnetic field is applied, the moment strengthens and the inverse happens. Therefore, the changes in lattice upon application of a field provide information about the magnetic contribution to the observed thermal expansion. In FeB, this magnetostructural coupling is small, so the thermal expansion is more or less unaffected by the magnetism. In MnB on the other hand, the anisotropic magnetoelastic effect modifies the standard thermal expansion. In the b direction, the magnetoeleastic effect is positive and large, which overwhelms the standard positive thermal expansion and leads to a strong negative thermal expansion. In the a direction, the negative magnetoelastic effect strengthens the positive thermal expansion leading to an exceptionally large positive thermal expansion. In the c direction, the weaker positive effect offsets the thermal expansion leading to a fairly temperature-independent lattice parameter, as is the case in invar.

Competing Interactions and Magnetostructural Coupling

In order to understand the origins of the unconventional thermal expansion and magnetoelastic effect in MnB, we employ density functional theory (DFT) calculations on both MnB and FeB. Noting that the strongest bonds in the system are the covalent B–B bonds which run in a zig-zag chain along the b lattice parameter, we show the results of DFT calculations for FeB and MnB unit cells with expanded and contracted b lattice parameters in Figure 7. B–B bond strength (as indicated by the integrated Crystal Orbital Hamilton Population, $-$iCOHP), Mn or Fe moment magnitude, and magnetic stabilization energy ($E_{\mathrm{mag}} - E_{\mathrm{nonmag}}$) are shown. In both compounds, contraction of the b lattice parameter

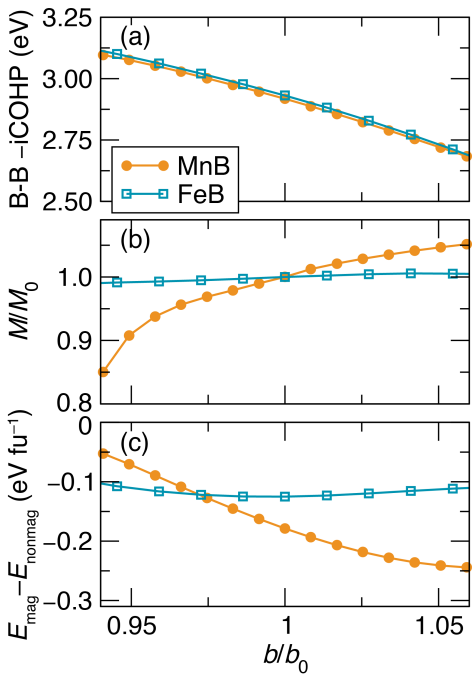

Figure 7: Results of DFT calculations for MnB and FeB cells with contracted and expanded b lattice parameter. (a) Integrated crystal orbital Hamilton population (iCOHP) between B–B atoms in the chain, an indicator of the bond strength, with more negative values indicating greater stability. (b) Evolution of the local moment magnitudes (normalized to their equilibrium values M_0), which decrease as b is contracted in MnB but stay constant in FeB. Similarly, (c) shows that the energy stabilization from magnetization (difference in energy between a spin-polarized and non-spin-polarized calculations) decreases as b is contracted in MnB, but stays constant in FeB. These results demonstrate that MnB displays direct competition between Mn moment formation and B–B bond formation, while FeB does not.

(up to about 20%) leads to an increase in the B–B bond strength, indicating that the B–B are more elongated than they would prefer to be, absent of other forces in the structure. On the other hand, contraction of the b lattice parameter leads to a decrease in moment magnitude and magnetic stabilization in MnB, indicating that the manganese magnetism would favor an expanded b lattice parameter. Therefore, the equilibrium lattice parameter in MnB can be understood as resulting from the result of a competition between moment magnitude and B–B bond strength. In FeB, on the other hand, the moment size and magnetic stabilization are virtually independent of b-lattice parameter, and no such competition exists.

We propose that it is the competition between stabilizing the magnetism and the bonding in MnB that leads to the strong and anisotropic magnetoelastic coupling. As temperature is increased and magnetic fluctuations set in, the magnetic stabilization weakens and the B–B bonds are able to exert their contractive forces on the structure, leading to negative thermal expansion in the b direction and a decrease in the B-B bond length and the closest Mn-B bond length. In this picture, the a lattice parameter responds to the driving forces in the b lattice direction with a positive Poisson ratio, alleviating some of the volumetric strain associated with the large decrease in b lattice parameter. This causes the negative magnetoelastic effect in the a direction. The c lattice direction is intermediate between these two cases since the B–B zigzag chains sit mostly in the b-c plane. In addition to explaining the thermal evolution of the lattice parameters, the competition-induced magnetostructural coupling in MnB can explain its extraordinary magnetocaloric effect. Because MnB sits in an active balance between magnetic and structural degrees of freedom, changes in magnetism or b lattice parameter can energetically compensate each other. This provides a low energy pathway for changing Mn moment magnitude, allowing a small stimulus (magnetic field) to cause a large change in magnetic state and therefore magnetic entropy.

FeB has a smaller transition metal cation than than MnB, due to the increased nuclear charge as well as the lower magnetic moment. Comparing the room-temperature crystal structures, the unit cell volume and metal-B bond lengths are all larger in MnB than in FeB. However, the b lattice parameter and B–B bond lengths only show a small increase, suggesting that the larger size of MnB is straining against the available size of the metal site in the FeB structure, which is constrained by the strong B–B bonding. In fact, MnB sits at a phase boundary: moving one column to the left on the periodic table yields CrB, a transition metal monoboride with a modified structure (space group $Cmcm$) from the $Pnma$ structure of the common forms of MnB, FeB, and CoB. In fact, MnB itself can be stabilized in either the $Pnma$ (as studied presently) or a low-temperature $Cmcm$ struc-

ture.[56] Therefore, we expect that FeB does not show the moment-bonding competition, and associated magnetostructural coupling that MnB does because the smaller size of the Fe atoms is not straining the B–B bonds.

Conclusion

We have demonstrated that MnB shows anisotropic magnetoelastic coupling that is driven by competition between Mn moment formation and B–B bond strength. These results explain why MnB shows a large magnetocaloric effect of $-10.7\,\mathrm{J\,Kg^{-1}K^{-1}}$ at 5 T, while isostructural FeB with otherwise similar magnetic properties shows a much smaller effect. While there is no change in the space group across the magnetic transition in MnB, coupling of magnetism and structure is evidently an important driver of the magnetocaloric performance. Based on this result, MnB appears to be proximal to a magnetostructural tricritical point which allows for a transition with a large ΔS_M while maintaining negligible hysteresis.

In addition, we have shown that the magnetic transition in MnB is in fact very subtly first-order with clear phase-coexistence at the magnetic transition, albeit the behavior of the transition is quite distinct from the giant first-order coupled magnetostructural transitions displayed by other magnetocalorics.

Supporting Information

Additional details of the temperature- and field-dependent Rietveld refinements, additional magnetization data, and example data from the in-field diffractometer.

Acknowledgements

This work was supported by the National Science Foundation (NSF) through DMR-1710638. Partial support by the NSF MRSEC Program under DMR 1720256 (IRG-1) is acknowledged. J.D.B. is supported by the NSF Graduate Research Fellowship Program under 1650114. We also acknowledge the use of the facilities of the Center for Scientific Computing at UC Santa Barbara. Use of the Advanced Photon Source at Argonne National Laboratory was supported by the U. S. Department of Energy, Office of Science, Office of Basic Energy Sciences, under Contract No. DE-AC02-06CH11357. We thank Dr. Saul Lapidus (Beamline 11-BM) for assistance with the data collection and Professor Dr. Barbara Albert for helpful discussions on the subject of borides.

References

(1) Wada, H.; Tanabe, Y. Giant magnetocaloric effect of $MnAs_{1-x}Sb_x$. *Appl. Phys. Lett.* **2001**, *79*, 3302.

(2) Mira, J.; Rivadulla, F.; Rivas, J.; Fondado, A.; Guidi, T.; Caciuffo, R.; Carsughi, F.; Radaelli, P.; Goodenough, J. Structural transformation induced by magnetic field and "colossal-like" magnetoresistance response above 313 K in MnAs. *Phys. Rev. Lett.* **2003**, *90*, 097203.

(3) Guo, Z.; Du, Y.; Zhu, J.; Huang, H.; Ding, W.; Feng, D. Large magnetic entropy change in perovskite-type manganese oxides. *Phys. Rev. Lett.* **1997**, *78*, 1142.

(4) Pecharsky, V. K.; Gschneidner, Jr., K. A. Giant magnetocaloric effect in $Gd_5(Si_2Ge_2)$. *Phys. Rev. Lett.* **1997**, *78*, 4494.

(5) Choe, W.; Pecharsky, V. K.; Pecharsky, A. O.; Gschneidner, K. A.; Young, V. G.; Miller, G. J. Making and breaking covalent bonds across the magnetic transition in the giant magnetocaloric material $Gd_5(Si_2Ge_2)$. *Phys. Rev. Lett.* **2000**, *84*, 4617.

(6) Choe, W.; Miller, G. J.; Meyers, J.; Chumbley, S.; Pecharsky, A. O. "Nanoscale zippers" in the crystalline Solid. Structural variations in the giant magnetocaloric material $Gd_5Si_{1.5}Ge_{2.5}$. *Chem. Mater.* **2003**, *15*, 1413–1419.

(7) Miller, G. J. Complex rare-earth tetrelides, $RE_5(Si_xGe_{1-x})_4$: New materials for magnetic refrigeration and a superb playground for solid state chemistry. *Chem. Soc. Rev.* **2006**, *35*, 799–813.

(8) Yao, J.; Wang, P.; Mozharivskyj, Y. Tuning magnetic and structural transitions through valence electron concentration in the giant magnetocaloric $Gd_{5-x}Eu_xGe_4$ Phases. *Chem. Mater.* **2012**, *24*, 552–556.

(9) Tegus, O.; Brück, E.; Buschow, K. H. J.; de Boer, F. R. Transition-metal-based magnetic refrigerants for room-temperature applications. *Nature* **2002**, *415*, 150.

(10) Brück, E.; Tegus, O.; Zhang, L.; Li, X.; de Boer, F.; Buschow, K. Magnetic refrigeration near room temperature with Fe_2P-based compounds. *J. Alloys Compd.* **2004**, *383*, 32.

(11) Cam Thanh, D. T.; Brück, E.; Trung, N. T.; Klaasse, J. C. P.; Buschow, K. H. J.; Ou, Z. Q.; Tegus, O.; Caron, L. Structure, magnetism, and magnetocaloric properties of $MnFeP_{1-x}Si_x$ compounds. *J. Appl. Phys.* **2008**, *103*, 07B318.

(12) Boeije, M. F. J.; Roy, P.; Guillou, F.; Yibole, H.; Miao, X. F.; Caron, L.; Banerjee, D.; van Dijk, N. H.; de Groot, R. A.; Brück, E. Efficient room-temperature cooling with magnets. *Chem. Mater.* **2016**, *28*, 4901–4905.

(13) Grebenkemper, J. H.; Bocarsly, J. D.; Levin, E. E.; Seward, G.; Heikes, C.; Brown, C.; Misra, S.; Seeler, F.; Schierle-Arndt, K.; Wilson, S. D.; Seshadri, R. Rapid microwave preparation and composition tuning of the high-performance magnetocalorics $(Mn,Fe)_2(P,Si)$. *ACS Appl. Mater. Interfaces* **2018**, *10*, 7208.

(14) Fujieda, S.; Fujita, A.; Fukamichi, K. Large magnetocaloric effect in $La(Fe_xSi_{1-x})_{13}$ itinerant-electron metamagnetic compounds. *Appl. Phys. Lett.* **2002**, *81*, 1276.

(15) Shen, B.; Sun, J.; Hu, F.; Zhang, H.; Cheng, Z. Recent progress in exploring magnetocaloric materials. *Adv. Mater.* **2009**, *21*, 4545.

(16) Brown, G. V. Magnetic heat pumping near room temperature. *J. Appl. Phys.* **1976**, *47*, 3673.

(17) Kishore, R. A.; Priya, S. A review on design and performance of thermomagnetic devices. *Renewable Sust. Ener. Rev.* **2018**, *81*, 33.

(18) Christiaanse, T.; Brück, E. Proof-of-concept static thermomagnetic generator experimental device. *Metall. Mater. Trans. E* **2014**, *1*, 36.

(19) Kishore, R. A.; Priya, S. Low-grade waste heat recovery using the reverse magnetocaloric effect. *Sustain. Energ. Fuels* **2017**, *1*, 1.

(20) Dung, N. H.; Zhang, L.; Ou, Z. Q.; Brck, E. From first-order magneto-elastic to magneto-structural transition in $(Mn,Fe)_{1.95}P_{0.50}Si_{0.50}$ compounds. *Appl. Phys. Lett.* **2011**, *99*, 092511.

(21) Guillou, F.; Porcari, G.; Yibole, H.; van Dijk, N.; Brück, E. Taming the first-order transition in giant magnetocaloric materials. *Adv. Mater.* **2014**, *26*, 2671.

(22) Gottschall, T.; Skokov, K. P.; Frincu, B.; Gutfleisch, O. Large reversible magnetocaloric effect in Ni-Mn-In-Co. *Appl. Phys. Lett.* **2015**, *106*, 021901.

(23) Gutfleisch, O.; Gottschall, T.; Fries, M.; Benke, D.; Radulov, I.; Skokov, K. P.; Wende, H.; Gruner, M.; Acet, M.; Entel, P.; Farle, M. Mastering hysteresis in magnetocaloric materials. *Philos. Trans. R. Soc. A* **2016**, *374*, 20150308.

(24) Franco, V.; Law, J. Y.; Conde, A.; Brabander, V.; Karpenkov, D. Y.; Radulov, I.; Skokov, K.; Gutfleisch, O. Predicting the tricritical point composition of a series of LaFeSi magnetocaloric alloys via universal scaling. *J. Phys. D* **2017**, *50*, 414004.

(25) Takeuchi, I.; Sandeman, K. Solid-state cooling with caloric materials. *Phys. Today* **2015**, *68*, 48.

(26) Boeije, M. F. J.; Maschek, M.; Miao, X. F.; Thang, N. V.; van Dijk, N. H.; Brück, E. Mixed magnetism in magnetocaloric materials with first-order and second-order magnetoelastic transitions. *J. Phys. D* **2017**, *50*, 174002.

(27) Law, J. Y.; Franco, V.; Moreno-Ramírez, L. M.; Conde, A.; Karpenkov, D. Y.; Radulov, I.; Skokov, K. P.; Gutfleisch, O. A quantitative criterion for determining the order of magnetic phase transitions using the magnetocaloric effect. *Nat. Commun.* **2018**, *9*, 2680.

(28) Mandal, K.; Yan, A.; Kerschl, P.; Handstein, A.; Gutfleisch, O.; Müller, K. The study of magnetocaloric effect in R_2Fe_{17} (R = Y, Pr) alloys. *J. Phys. D* **2004**, *37*, 2628.

(29) Singh, S.; Caron, L.; D'Souza, S. W.; Fichtner, T.; Porcari, G.; Fabbrici, S.; Shekhar, C.; Chadov, S.; Solzi, M.; Felser, C. Large magnetization and reversible magnetocaloric effect at the second-order magnetic transition in heusler materials. *Adv. Mater.* **2016**, *28*, 3321.

(30) Sandeman, K. G. Magnetocaloric materials: The search for new systems. *Scr. Mater.* **2012**, *67*, 566.

(31) Tan, X.; Chai, P.; Thompson, C. M.; Shatruk, M. Magnetocaloric effect in $AlFe_2B_2$: Toward magnetic refrigerants from earth-abundant elements. *J. Am. Chem. Soc.* **2013**, *135*, 9553.

(32) Barua, R.; Lejeune, B.; Jensen, B.; Ke, L.; McCallum, R.; Kramer, M.; Lewis, L. Enhanced room-temperature magnetocaloric effect and tunable magnetic response in Ga-and Ge-substituted $AlFe_2B_2$. *J. Alloys Compd.* **2019**, *777*, 1030.

(33) Songlin,; Dagula,; Tegus, O.; Brück, E.; de Boer, F.; Buschow, K. Magnetic and magnetocaloric properties of $Mn_5Ge_{3-x}Sb_x$. *J. Alloys Compd.* **2002**, *337*, 269.

(34) Zhang, X.; Chen, Y.; Lü, L.; Li, Z. A potential oxide for magnetic refrigeration application: CrO_2 particles. *J. Phys. Condens. Matter* **2006**, *18*, L559.

(35) Bocarsly, J. D.; Levin, E. E.; Garcia, C. A. C.; Schwennicke, K.; Wilson, S. D.; Seshadri, R. A simple computational proxy for screening magnetocaloric compounds. *Chem. Mater.* **2017**, *29*, 1613.

(36) Fries, M.; Gercsi, Z.; Ener, S.; Skokov, K. P.; Gutfleisch, O. Magnetic, magnetocaloric and structural properties of manganese based monoborides doped with iron and cobalt – A candidate for thermomagnetic generators. *Acta Mater.* **2016**, *113*, 213.

(37) Elliott, J. F.; Legvold, S.; Spedding, F. H. Some magnetic properties of gadolinium metal. *Phys. Rev.* **1953**, *91*, 28–30.

(38) Shigematsu, T.; Kanaizuka, T.; Kosuge, K.; Shiga, M.; Nakamura, Y.; Kachi, S. Thermal expansion anomaly of MnB. *Phys. Lett. A* **1975**, *53*, 385.

(39) Kanaizuka, T. Invar like properties of transition metal monoborides $Mn_{1-x}Cr_xB$ and $Mn_{1-x}Fe_xB$. *Mater. Res. Bull.* **1981**, *16*, 1601.

(40) Park, J.; Hong, Y.-K.; Kim, H.-K.; Lee, W.; Yeo, C.-D.; Kim, S.-G.; Jung, M.-H.; Choi, C.-J.; Mryasov, O. N. Electronic structures of MnB soft magnet. *AIP Advances* **2016**, *6*, 055911.

(41) Gueddouh, A. The effects of magnetic moment collapse under high pressure, on physical properties in mono-borides TMB (TM = Mn, Fe): A first-principles. *Phase Transitions* **2017**, *1594*, 1.

(42) Ma, S.; Bao, K.; Tao, Q.; Zhu, P.; Ma, T.; Liu, B.; Liu, Y.; Cui, T. Manganese mono-boride, an inexpensive room temperature ferromagnetic hard material. *Sci. Rep.* **2017**, *7*, 43759.

(43) Stickel, J. J. Data smoothing and numerical differentiation by a regularization method. *Computers Chem. Eng.* **2010**, *34*, 467.

(44) Bocarsly, J. D.; Need, R. F.; Seshadri, R.; Wilson, S. D. Magnetoentropic signatures of skyrmionic phase behavior in FeGe. *Phys. Rev. B* **2018**, *97*, 100404.

(45) Stinton, G. W.; Evans, J. S. O. Parametric Rietveld refinement. *J. Appl. Crystallogr.* **2007**, *40*, 87.

(46) Faske, T.; Donner, W. X-ray diffractometer for the investigation of temperature- and magnetic field-induced structural phase transitions. *J. Appl. Crystallogr.* **2018**, *51*, 761.

(47) Kresse, G.; Furthmüller, J. Efficient iterative schemes for ab initio total-energy calculations using a plane-wave basis set. *Phys. Rev. B* **1996**, *54*, 11169–11186.

(48) Blöchl, P. E. Projector augmented-wave method. *Phys. Rev. B* **1994**, *50*, 17953.

(49) Kresse, G.; Joubert, D. From ultrasoft pseudopotentials to the projector augmented-wave method. *Phys. Rev. B* **1999**, *59*, 1758.

(50) Perdew, J. P.; Burke, K.; Ernzerhof, M. Generalized Gradient Approximation Made Simple. *Phys. Rev. Lett.* **1996**, *77*, 3865.

(51) Dronskowski, R.; Bloechl, P. E. Crystal orbital Hamilton populations (COHP): Energy-resolved visualization of chemical bonding in solids based on density-functional calculations. *J. Phys. Chem.* **1993**, *97*, 8617.

(52) Deringer, V. L.; Tchougréeff, A. L.; Dronskowski, R. Crystal orbital Hamilton population (COHP) analysis as projected from plane-wave basis sets. *J. Phys. Chem. A.* **2011**, *115*, 5461.

(53) Maintz, S.; Deringer, V. L.; Tchougréeff, A. L.; Dronskowski, R. Analytic projection from plane-wave and PAW wavefunctions and application to chemical-bonding analysis in solids. *J. Comp. Chem.* **2013**, *34*, 2557.

(54) Maintz, S.; Deringer, V. L.; Tchougréeff, A. L.; Dronskowski, R. LOBSTER: A tool to extract chemical bonding from plane-wave based DFT. *J. Comp. Chem.* **2016**, *37*, 1030.

(55) Maintz, S.; Esser, M.; Dronskowski, R. Efficient rotation of local basis functions using real spherical harmonics. *Acta Phys. Polon. B* **2016**, *47*, 1165.

(56) Kanaizuka, T. Phase diagram of pseudobinary CrB–MnB and MnB–FeB systems: Crystal structure of the low-temperature modification of FeB. *J. Solid State Chem.* **1982**, *41*, 195.

(57) Mohn, P.; Pettifor, D. The calculated electronic and structural properties of the transition-metal monoborides. *Journal of Physics C: Solid State Physics* **1988**, *21*, 2829.

(58) Stephens, P. W. Phenomenological model of anisotropic peak broadening in powder diffraction. *J. Appl. Crystallogr.* **1999**, *32*, 281.

(59) Gottschall, T.; Benke, D.; Fries, M.; Taubel, A.; Radulov, I. A.; Skokov, K. P.; Gutfleisch, O. A matter of size and stress: Understanding the first-order transition in materials for solid-state refrigeration. *Adv. Funct. Mater.* **2017**, *27*, 1606735.

(60) Wohlfarth, E. Thermodynamic aspects of itinerant electron magnetism. *Physica B+C* **1977**, *91*, 305.

(61) Moriya, T.; Usami, K. Magneto-volume effect and invar phenomena in ferromagnetic metals. *Solid State Commun.* **1980**, *34*, 95.

(62) Huang, R.; Liu, Y.; Fan, W.; Tan, J.; Xiao, F.; Qian, L.; Li, L. Giant negative thermal expansion in $NaZn_13$-type La(Fe,Si,Co)$_13$ compounds. *J. Am. Chem. Soc.* **2013**, *135*, 11469–11472.

(63) Hu, F.; Shen, F.; Hao, J.; Liu, Y.; Wang, J.; Sun, J.; Shen, B. Negative thermal expansion in the materials with giant magnetocaloric effect. *Front. Chem.* **2018**, *6*, 438.

Graphical TOC Entry

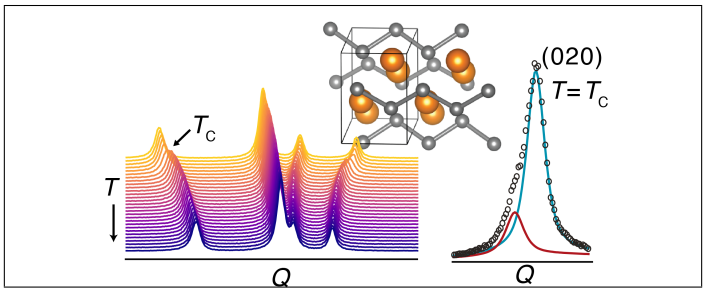

Supporting Information for

Magnetostructural Coupling Drives Magnetocaloric Behavior: The Case of MnB *versus* FeB

Joshua D. Bocarsly,[†,‡] Emily E. Levin,[†,‡] Samuel A. Humphrey,[¶] Tom Faske,[§] Wolfgang Donner,[§] Stephen D. Wilson,[†,‡] and Ram Seshadri[*,†,‖,‡]

†*Materials Department*

University of California, Santa Barbara, California 93106, United States

‡*Materials Research Laboratory*

University of California, Santa Barbara, California 93106, United States

¶*Department of Materials*

University of Oxford, Oxford OX1 3PH, United Kingdom

§*Department of Materials and Earth Sciences, Technische Universität Darmstadt, Darmstadt 64287, Germany.*

‖*Department of Chemistry and Biochemistry*

University of California, Santa Barbara, California 93106, United States

E-mail: seshadri@mrl.ucsb.edu

Table S1: Refined crystal structure of MnB and FeB from room temperature high-resolution synchrotron diffraction data (λ=0.414581 Å). GOF indicates the goodness of fit, which is defined as the ratio between the weighted profile R factor R_{wp}, and expected R factor, R_{exp}. Numbers in parentheses are standard uncertainties in the last given digit(s) from Rietveld refinement. The refined structures are also included in Crystallographic Information Files.

	MnB (300 K)	FeB (300 K)
spacegroup	$Pnma$	$Pnma$
a (Å)	5.5632	5.5020
b (Å)	2.9769	2.9482
c (Å)	4.1473	4.0596
V (Å)^3	68.682	65.852
GOF	1.93	1.57
metal		
x	0.17588(2)	0.17709(3)
y	0.25	0.25
z	0.12083(3)	0.11988(4)
B_{iso}	0.158(2)	0.162(2)
boron		
x	0.0341(2)	0.0363(2)
y	0.25	0.25
z	0.6128(3)	0.6141(3)
B_{iso}	0.35(1)	0.29(1)

Table S2: Refined lattice parameters and weight fractions for the high-temperature phase of MnB from the temperature-dependent synchrotron diffraction data. Numbers in parentheses are standard uncertainties in the last given digit(s) from Rietveld refinement. The values for temperatures from 590.1 K to 580.1 K are from the single-phase parametric refinement, while the values for temperatures between 577.0 K and 557.7 K are from the two-phase parametric refinement, with the lattice parameters and weight fractions for the other (low temperature) phase given in Table S3.

T	a (Å)	b (Å)	c (Å)	V (Å)	weight fraction (%)
590.1	5.60293(1)	2.96463(1)	4.15299(1)	68.9836(1)	100
586.6	5.60221(1)	2.96490(1)	4.15287(1)	68.9790(1)	100
583.3	5.60149(1)	2.96522(1)	4.15278(1)	68.9761(1)	100
580.1	5.60059(1)	2.96566(1)	4.15272(1)	68.9744(1)	100
577.0	5.60014(1)	2.96586(1)	4.15300(1)	68.9781(2)	77.0(3)
573.8	5.59912(2)	2.96646(1)	4.15306(1)	68.9805(3)	59.0(3)
570.5	5.59771(3)	2.96742(2)	4.15314(2)	68.9868(6)	43.3(4)
567.7	5.59668(4)	2.96811(3)	4.15335(2)	68.9936(9)	27.2(5)
564.3	5.59596(6)	2.96865(4)	4.15353(3)	69.000(1)	18.7(5)
561.1	5.59536(7)	2.96909(5)	4.15355(4)	69.003(2)	13.4(4)
557.7	5.59492(8)	2.96977(5)	4.15181(5)	68.985(2)	10.3(4)

Table S3: Lattice parameters and weight fractions refined for the low-temperature phase of MnB from the temperature-dependent synchrotron diffraction data. The values for temperatures from 577.0 K to 557.7 K are from the two-phase parametric refinement, with the lattice parameters and weight fractions for the other (high-temperature) phase given in Table S2. The values for temperatures from 554.3 K to 500.0 K are from the single-phase parametric refinement.

T	a (Å)	b (Å)	c (Å)	V (Å)	weight fraction (%)
577.0	5.59729(3)	2.96794(1)	4.15204(2)	68.9754(5)	23.0(3)
573.8	5.59619(2)	2.96834(1)	4.15252(1)	68.9791(3)	41.0(3)
570.5	5.59505(2)	2.96894(1)	4.15276(1)	68.9829(3)	56.7(4)
567.7	5.59400(1)	2.96952(1)	4.15280(1)	68.9842(3)	72.8(5)
564.3	5.59307(1)	2.97005(1)	4.15288(1)	68.9866(2)	81.3(5)
561.1	5.59215(1)	2.97051(1)	4.15289(1)	68.9859(2)	86.6(4)
557.7	5.59126(1)	2.97096(1)	4.15303(1)	68.9876(2)	89.7(4)
554.3	5.59070(1)	2.97130(1)	4.15296(1)	68.9876(1)	100
551.5	5.58991(1)	2.97163(1)	4.15291(1)	68.9845(1)	100
548.0	5.58914(1)	2.97196(1)	4.15286(1)	68.9820(1)	100
545.0	5.58845(1)	2.97227(1)	4.15282(1)	68.9798(1)	100
541.6	5.58782(1)	2.97253(1)	4.15278(1)	68.9775(1)	100
538.4	5.58718(1)	2.97278(1)	4.15272(1)	68.9743(1)	100
535.3	5.58656(1)	2.97300(1)	4.15265(1)	68.9707(1)	100
532.1	5.58601(1)	2.97321(1)	4.15261(1)	68.9682(1)	100
528.7	5.58547(1)	2.97343(1)	4.15256(1)	68.9658(1)	100
525.6	5.58499(1)	2.97362(1)	4.15253(1)	68.9636(1)	100
522.3	5.58443(1)	2.97376(1)	4.15243(1)	68.9584(1)	100
519.1	5.58393(1)	2.97393(1)	4.15237(1)	68.9550(1)	100
516.1	5.58345(1)	2.97409(1)	4.15233(1)	68.9524(1)	100
512.5	5.58301(1)	2.97426(1)	4.15228(1)	68.9498(1)	100
509.7	5.58248(1)	2.97437(1)	4.15218(1)	68.9443(1)	100
506.5	5.58202(1)	2.97450(1)	4.15210(1)	68.9404(1)	100
503.3	5.58159(1)	2.97463(1)	4.15204(1)	68.9371(1)	100
500.0	5.58140(1)	2.97470(1)	4.15202(1)	68.9359(1)	100

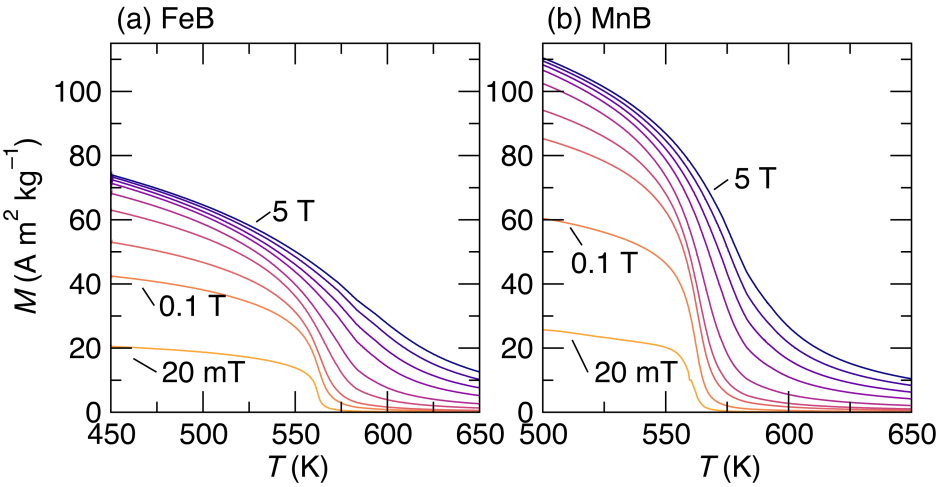

Figure S1: Magnetization *vs.* temperature under a nine applied fields for FeB (a), and MnB (b). These data are processed into the ΔS_M data presented in the main text Figure 2. At high field, the FeB $M(T)$ broadens out considerably while the MnB remains relatively sharp, leading to a much larger peak ΔS_M for MnB.

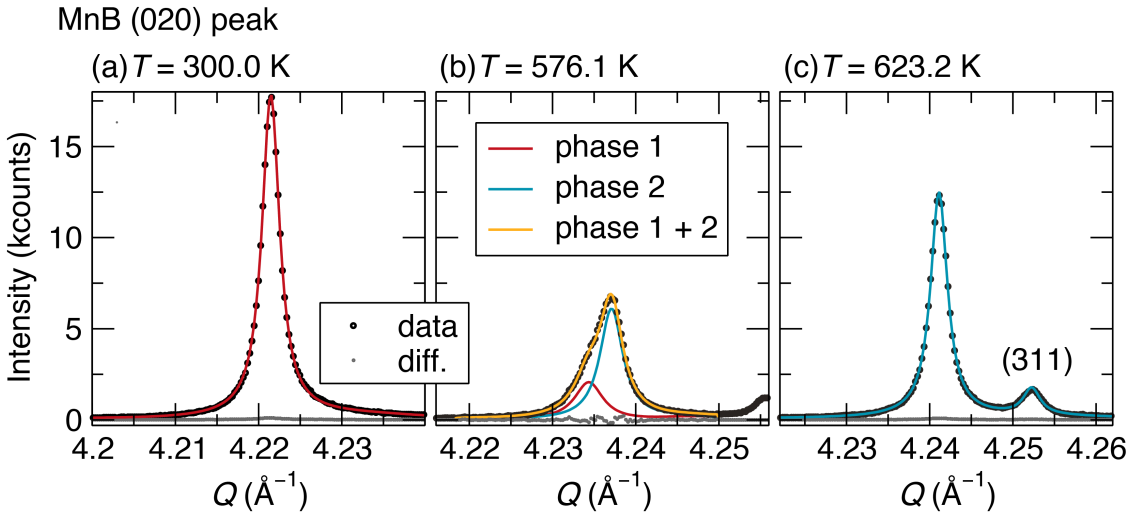

Figure S2: MnB (020) synchrotron diffraction peak from patterns taken while equilibrated at temperatures well below the magnetic transition (a), near the magnetic transition (b), and well-above the magnetic transition (c). This data is similar to the data in the main text Figure 4, except that these patterns are taken at static temperature after temperature equilibration. In (a) and (c), the diffraction peaks can be fit with a single Lorentzian peak, while around the magnetic transition two Lorentzians are required, indicating phase coexistence of two phases.

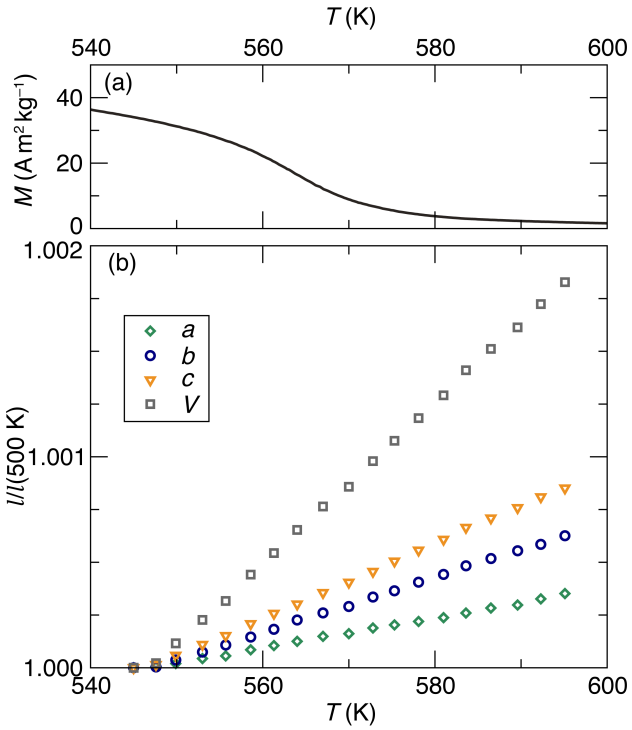

Figure S3: Comparison of magnetic moment *vs.* temperature (a) and lattice parametric from parametric Rietveld refinement of temperature-dependent synchrotron diffraction data (b) for FeB. In contrast to MnB (main text Figure 5), the lattice parameters of FeB all show linear, moderate positive thermal expansion, with no obvious anomaly at the magnetic transition temperature. Some anisotropy in thermal expansion can be seen, evidenced by a larger coefficient of thermal expansion in the c direction than the a and b direction.

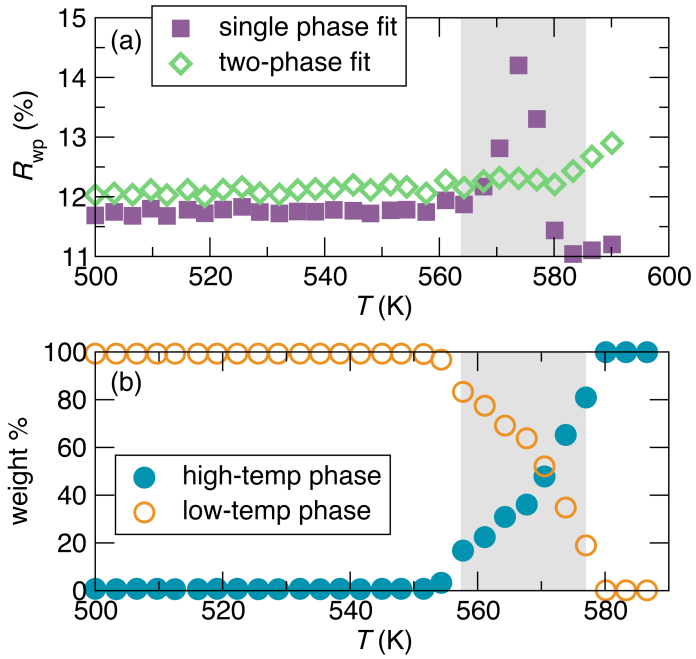

Figure S4: (a) Quality of fit (R_{wp}) for parametric fit of temperature-dependent synchrotron diffraction data. The purple squares show that case when a single crystallographic phase is allowed, with the peak profile (Bragg peak widths) allowed to vary independently for each pattern. This case cannot adequately fit the Bragg peak splitting observed near the magnetic transition temperature, and a spike in R_{wp} is observed in the grey boxed region. On the other hand, when two phases with slightly different lattice parameters and each with a constant peak profile are included, the R_{wp} is constant through the magnetic transition. The weight fractions of the two phases refined from this fit are shown in (b), demonstrating that the magnetic transition is concurrent with the conversion from one crystallographic phase to the other, confirming a first-order transition.

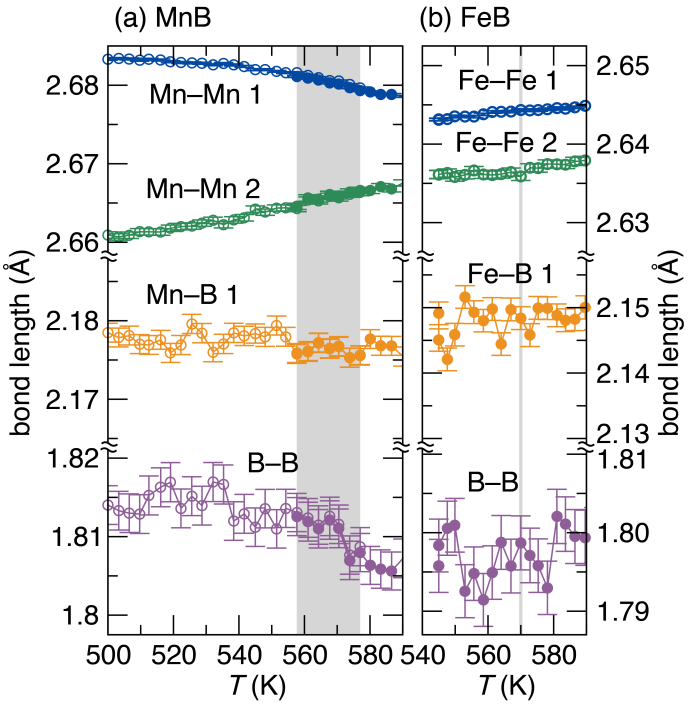

Figure S5: Thermal evolution of selected bond lengths and contacts in MnB and FeB, as fit from the parametric refinements. For MnB, the high-temperature phase is indicated with solid symbols, and the low-temperature phase with empty symbols. The atomic positions were constrained to be the same in the two phases for the patterns where both phases exist, which is consistent with the positions above and below the transition. In each compound, there exist two distinct metal-metal contacts with length below 2.7 Å, seven distinct metal-boron contacts with length less than 2.3 Å(only the nearest is shown), and one distinct boron-boron contact. MnB shows anisotropic thermal expansion of its bonds, while FeB shows only mild increases in bond length as temperature is raised. Magnetic transition temperatures are represented as grey box for MnB (signifying the temperature range of phase co-existence), and a grey line for FeB.

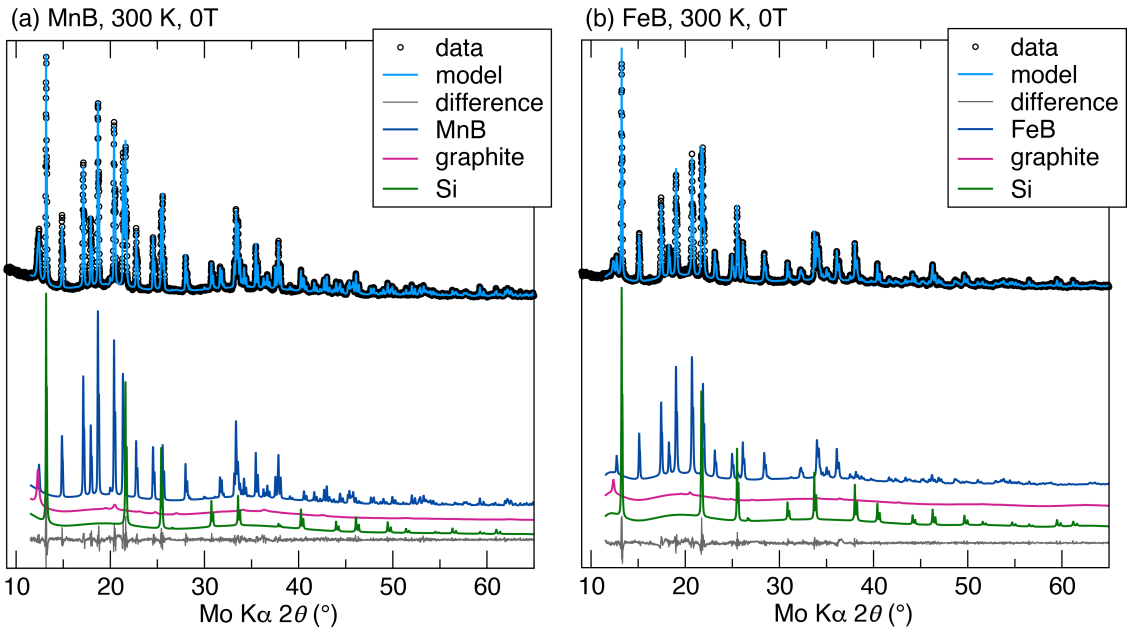

Figure S6: Example Pawley fits of the diffraction data from the in-field, variable temperature X-ray diffractometer (in this case, taken at 300 K with no applied field). The samples (single phase MnB or FeB) have been mixed with NIST 640D standard reference silicon and mounted on a graphite support. Both silicon and graphite phases are included in the Pawley refinement, and the known silicon lattice parameter is used to correct instrumental geometric errors.

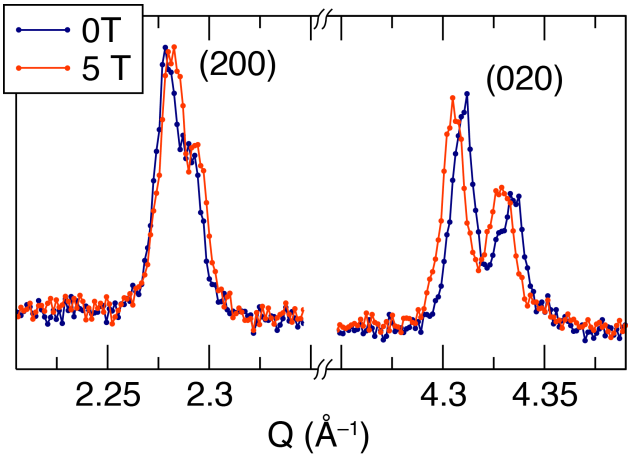

Figure S7: Detailed view of the difference in MnB diffraction pattern under zero applied field and 5 T applied field, taken at 600 K. Only the (200) and (020) peaks are shown. The doublet peaks are from Mo Kα_1 and Kα_2 radiation. Upon application of the field, an anisotropic magneto-elastic effect is seen, with some lattice peaks with substantial h character moving to the right, and lattice peaks with substantial k character moving to the left. The full patterns (along with those taken at other fields) were fitted to give the data shown in the main text Figure 6c.

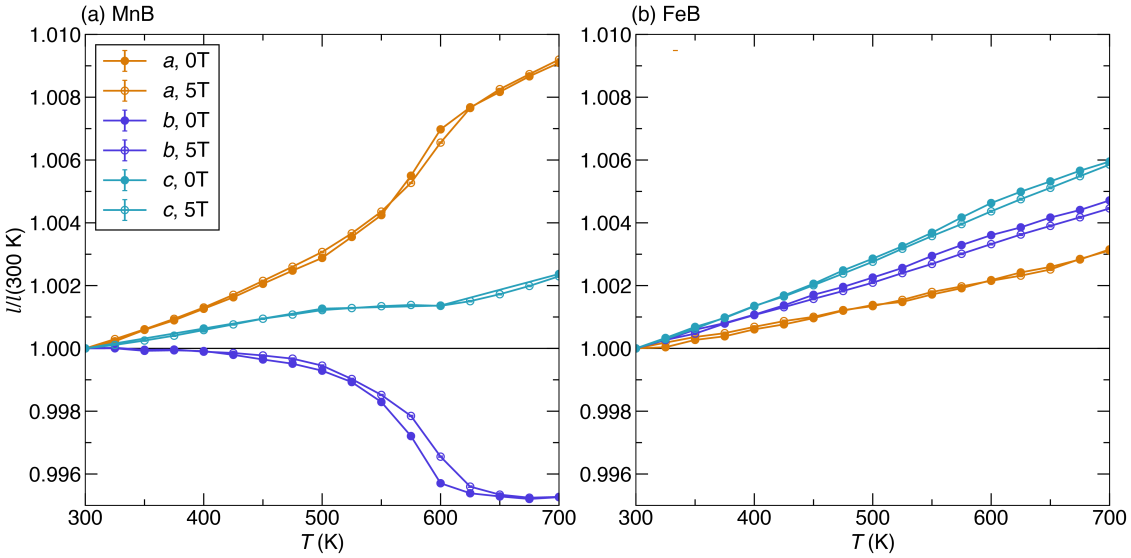

Figure S8: Lattice parameters fit from temperature and field-dependent XRD patterns of MnB and FeB, normalized to their 300 K values at zero field. These refinements were used to generate the induced magnetoelasticity (difference in lattice parameters upon application of a magnetic field) data shown in the main text, Figure 6. Due to a sample history effects observed in MnB in the c lattice parameter, c, 0 T data are fit from a later run, after the sample had been cycled to remove any history. Error bars, which are in general smaller than the data points, represent standard uncertainties from the Pawley refinements.